J. Webster (ed.), *Wiley Encyclopedia of Electrical and Electronics Engineering*


# RADAR SIGNAL PROCESSING

## Fundamentals of Radar Signal Processing

The capability of radar in acquiring information about targets and environments has been greatly improved over the decades, not only owing to the advent of sophisticated hardware, but also the development of advanced signal-processing techniques. Conventional radar is mainly used for detection, localization, and tracking of targets. High-resolution imaging radar can provide more information such as target size, shape, and image and hence can be used for target recognition, which is desired by modern radar. Signal processing plays a key role in most modern radar operations. *Radar signal processing* commonly refers to the techniques that are used to extract desired information about a target from the received signals. Such information usually includes target presence and the position, velocity, trajectory, and image of the target.

According to their objectives, the signal-processing techniques can be divided into two categories. The techniques in the first category are mainly used to enhance the useful signal and suppress interference, thus enabling the radar to work satisfactorily in less-than-ideal environments. The techniques in the second category are developed to improve the resolving capability of radar, thus enabling the radar to extract complex information, such as target size and shape.

**Signal Enhancement and Interference Suppression.** Extraction of desired information from radar echoes is not an easy task under most circumstances, since the wanted signal has to compete with unwanted signals, such as noise, clutter, and external interference. Noise includes thermal noise and other noiselike disturbances and errors introduced into the receiving channels of radar. It is normally modeled as a Gaussian random process with a uniform power spectrum (white). Clutter is the echo from targets of no interest. For example, if the target of interest is an aircraft, the echoes from the ground, clouds, and rain will produce clutter. Unlike that of noise, the spectrum of clutter is not uniform and is determined by the Doppler frequency and strength of the clutter source. External interference can be generated either by hostile jamming devices or other microwave equipment operating nearby. Radars usually operate in such a combined environment. Different techniques are required to suppress noise, clutter, and jamming since they have different properties.

We first consider coping with noise. In order to ensure reliable detection and processing, it is desirable to maximize the signal-to-noise ratio (*SNR*). The optimum filter that achieves the maximum *SNR* is the *matched filter*. The matched filter is widely used in radar systems and is often considered part of the radar receiver, because the intermediate-frequency (*IF*) amplifier in the radar receiver is normally designed as the matched filter. The matched filter is also an important element in pulse compression. The theory of matched filter is discussed in detail in another article in this encyclopedia, Radar signal detection This article briefly introduces the concept of matched filter.

Denote the input signal and its Fourier transform by $s(t)$ and $s(\omega)$, respectively. The input noise is assumed to be white and stationary. Its spectral density in watts/hertz is $N_0/2$. The frequency response of the matched

filter is (1)

$$H(\omega) = kS^*(\omega)\exp(-j\omega t_0) \qquad (1)$$

where the asterisk denotes the complex conjugate, $k$ is a gain constant, and $t_0$ is a time delay that makes the filter physically realizable. The impulse response of the matched filter is the inverse Fourier transform of Eq. (1), which is

$$h(t) = ks(t_0 - t) \qquad (2)$$

So the impulse response is the image or time inverse of the input signal.

The *SNR* used here is defined as the ratio of the peak instantaneous signal power and the average noise power. It is maximized at the output of the matched filter as $\mathrm{SNR}_{max}=2E/N_0$, where $E$ is the signal energy. It is an interesting fact that the output *SNR* is independent of the waveform shape of the input signal.

Clutter reduction is also a major concern for many radar applications. Moving target indication (*MTI*) is an important technique that can discriminate moving targets from fixed or slowly moving clutter. *MTI* is based on the phenomenon that the target moving with finite radial velocity produces a Doppler frequency whereas the fixed target does not. So the difference in Doppler frequency can be utilized to filter out the fixed clutter.

For radars operating in military environment, antijamming capability is a crucial performance indicator. In this case, the technique of frequency-domain filtering is ineffective, since the interfering signal usually has similar Doppler properties as the desired signal. However, a jamming source is confined to within a certain spatial angle and is usually not in the same direction as the target. So it can be removed by spatial filtering. The technique of spatial filtering is known as *beam forming*. By combining the signals of individual elements of a phased-array antenna, it can synthesize a beam pattern whose mainlobe points to the desired target and a very low sidelobe points to the jamming source.

However, no practical techniques can completely suppress these unwanted signals. The residual interference will lead to a higher false-alarm rate when a fixed threshold is used to decide the presence of a target. Having too many false alarms is unacceptable for the radar detector. Moreover, it also increases the computational load of subsequent data processors. Therefore, a device is needed to control the threshold adaptively in order to maintain an approximately constant false-alarm rate (*CFAR*).

**Improvement of Resolving Capability.** Radar has two main tasks: detection and information extraction. Early radar only has the capability to extract simple target information, such as range, angle, and velocity. Modern radar is able to acquire complicated information such as target size, shape, and image. This is largely a result of the advancement of radar signal processing. Extracting such information requires the radar to have high resolution in one or two (or even three) dimensions.

*Range resolution* is the ability of radar to distinguish adjacent targets in range direction. If the radar transmits a short pulse of single frequency, range resolution is decided by the pulse duration $T$. In this case, two scatterers adjacent in range can be distinguished by the radar if their echoes are separated in time delay by more than the pulse width. So the range resolution is

$$\rho_{\mathrm{r}} = cT/2 \qquad (3)$$

where $c$ is the speed of light and the factor 2 is introduced by the two-way time delay.

Thus, the shorter the pulse, the finer the range resolution. However, a very short pulse carries little energy, and it is impractical, if not impossible, to generate short pulses of very large amplitudes. Hence, a detection range would be shortened due to fixed *SNR* requirement of the receiver. To overcome this drawback, high-resolution radars usually adopt long-duration, wideband, coded pulses, which can be compressed to very short pulses after reception by an operation called *pulse compression*.

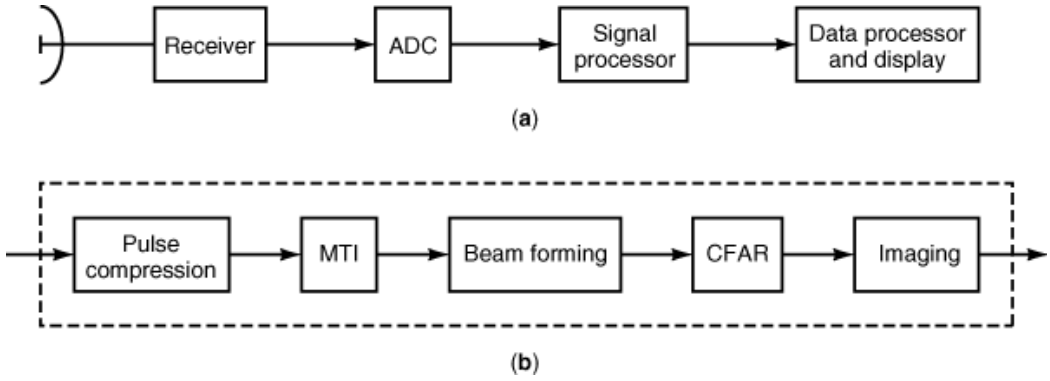


**Fig. 1.** (a) illustrates the position of the radar signal processor in the receiving and processing channel of a radar system. (b) shows an inside view of the radar signal processor. The configurations vary in practical processors.

High range resolution makes it possible for the radar to acquire information on target size and shape. On the other hand, if the target image is needed, the radar must have high resolution in the azimuth direction as well. For conventional radar, this corresponds to the angular resolution, which is actually the antenna beam width, because the radar can distinguish two scatterers in the azimuth only if their angular separation is greater than the antenna beam width. The beam width is decided by the ratio of the signal wavelength to the aperture size of the antenna. The larger the aperture, the sharper the beam.

However, it is usually impractical to increase the aperture size of a real antenna to a great extent. For instance, assuming a signal wavelength of 3 cm, a whopping 300-m antenna aperture is needed in order to resolve two targets located 1 m apart at a range of 10 km. The synthetic aperture radar (*SAR*) is developed to overcome this limitation. In *SAR*, the radar is installed on a moving platform, such as an aircraft or a satellite. The radar transmits and receives a series of pulses while moving with the platform. This is equivalent to obtaining discrete samples of a long aperture. The long antenna aperture can be synthesized by a coherent summation of these samples after proper phase adjustment. Thus, *SAR* achieves high resolution in azimuth in a practical way. It presents the image of the target by resolving the backscattering intensity of each small range-azimuth cell.

**Radar Signal Processor.** In a radar system, the device that performs the operations of radar signal processing is termed the *radar signal processor*. The radar signal processor is sometimes considered part of the radar receiver in early days. In modern radars, it incorporates more and more important functions and is usually considered a separate subsystem due to its significance.

Figure 1(a) shows the block diagram of the receiving and processing channel of the radar system. The receiver accepts radio frequency (*RF*) signals from the antenna and down-converts them to an intermediate frequency. The signals are then amplified, converted to video frequency (baseband), and sent to the analog-to-digital converter (*ADC*). The digital samples of the signals are the input to the signal processor. Finally, the output of the signal processor goes to the data processor and display devices.

Figure 1(b) gives an inside view of the radar signal processor, which encompasses all major functions of radar signal processing. The configurations of practical signal processors may vary according to the main function of radar. A typical signal processor usually does not contain all the components depicted in the block diagram, and may not incorporate them in the given order.

**Coherent Signal Processing.** Most functions of the radar signal processor require coherent processing, which means that both signal amplitudes and phases are utilized. Noncoherent processing only uses signal amplitudes. A device called *synchronous detector* or *phase-sensitive detector*, as shown in Fig. 2, obtains coherent

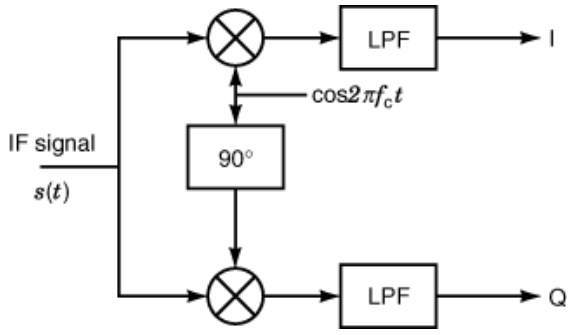


**Fig. 2.** The synchronous detector consists of two orthogonal channels, corresponding to the real and imaginary parts of a signal. Its output is a complex video signal.

video signals. It consists of two orthogonal channels denoted by I (in-phase) and Q (quadrature), which correspond to the real and imaginary part of a signal, respectively.

The input is usually an IF signal, which has the general form of

$$s(t) = A(t)\cos[2\pi f_c t + \phi(t)] \tag{4}$$

where $A(t)$ is the amplitude or envelope, $f_c$ is the IF frequency, and $\phi(t)$ is the phase. It is mixed with the following orthogonal signals in the two channels:

$$r_I(t) = \cos 2\pi f_c t, \qquad r_Q(t) = \sin 2\pi f_c t \tag{5}$$

The output of the multiplier in the I channel is

$$s(t)r_I(t) = (1/2)A(t)\cos[2\pi(2f_c)t + \phi(t)] + (1/2)A(t)\cos\phi(t) \tag{6}$$

The first term has a doubled frequency and is thus removed by the subsequent low-pass filter (*LPF*). The final output of the I channel is

$$I(t) = (1/2)A(t)\cos\phi(t) \tag{7}$$

Similarly, the output of the Q channel is

$$Q(t) = (1/2)A(t)\sin\phi(t) \tag{8}$$

The complex video signal can be reconstructed as

$$v(t) = 2[I(t) + jQ(t)] = A(t)\exp[j\phi(t)] \tag{9}$$

This complex signal is the so-called *complex envelope* of $s(t)$. It contains the information of the amplitude as well as the phase.

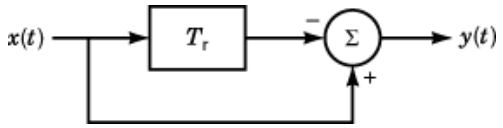


**Fig. 3.** The single canceler utilizes only two pulses. The delay time $T_r$ exactly equals one interpulse period.

## Moving-Target Indication

Discrimination of moving targets from strong, fixed clutter is necessary for many radar applications, for example, air surveillance and air traffic control. The *MTI* achieves this goal by means of the Doppler effect generated by a moving target. The transmitted signal is a series of pulses with a pulse repetition frequency (*PRF*) $f_r$. The Doppler frequency $f_D$ of a moving target will introduce a varying phase term into the received signal. The total phase of the received signal becomes

$$\phi(t) = 2\pi f_D t + \phi_0 \tag{10}$$

where $\phi_0$ is the initial phase. The output video signals of the synchronous detector are

$$x_I(t) = A(t)\cos(2\pi f_D t + \phi_0) \tag{11}$$

$$x_Q(t) = A(t)\sin(2\pi f_D t + \phi_0) \tag{12}$$

In the frequency domain, their spectra are centered at $\pm f_D$. On the other hand, a fixed target has zero Doppler frequency. The different spectral locations makes it possible to separate moving targets from fixed clutter.

The I or Q components or both can be used in the *MTI* process. If only one channel is used, the signal of a moving target may be lost in some special cases. For example, a moving target generating a Doppler frequency $f_D$ that equals half the sampling frequency may not be detected if the samples happened to fall at the zero crossings. Using both I and Q channels can overcome this problem. In this case, the signals of I and Q are fed into two separate *MTI* filters.

**Delay-Line Cancelers.** The delay-line canceler is a widely used form of MTI. Since the video signal of a fixed target does not vary from pulse to pulse, it can be subtracted using adjacent pulses. The *single canceler* is the simplest implementation of the MTI. Figure 3 shows its structure. The delay line therein introduces a delayed time that exactly equals one interpulse period, which is the reciprocal of the *PRF*, that is, $t_r = 1/f_r$. The single canceler utilizes only two pulses, and the output signal is

$$y(t) = x(t) - x(t - T_r) \tag{13}$$

The frequency response of a single canceler can be obtained via the Fourier transform of Eq. (13)

$$Y(\omega) = X(\omega) - X(\omega)\exp(-j\omega T_r) \tag{14}$$

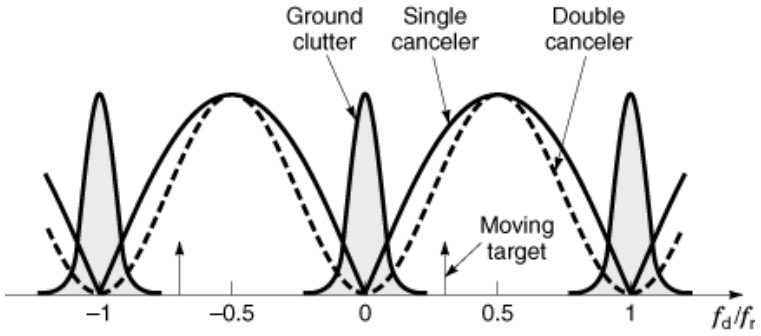


**Fig. 4.** The solid line is the frequency responses of the single canceler. It has rejection notches at zero Doppler frequency and $n f_r$, where $n$ is an integer. The double canceler, shown as the dashed line, provides broader notches and thus removes more clutter. Blind speed occurs when the Doppler frequency of the target equals $n f_r$.

where $\omega = 2\pi f_D$, since the frequency of the video signal is actually its Doppler frequency, as shown in Eqs. (11) and (12). So the frequency response of the single canceler is

$$H(\omega) = Y(\omega)/X(\omega) = 1 - \exp(-j\omega T_r) \tag{15}$$

The magnitude of the frequency response is

$$|H(\omega)| = 2\sin(\omega T_r/2) = 2\sin(\pi f_D/f_r) \tag{16}$$

Figure 4 shows the filtering mechanism of the delay-line canceler. The solid line is the magnitude of the frequency response of the single canceler. It forms notches at the zero Doppler frequency and the integer multiples of $f_r$. The moving target whose Doppler frequency is not zero will pass the filter.

The spectrum of completely fixed clutter is an impulse at zero Doppler frequency and can be removed by the single canceler. However, practical ground clutter usually has a finite spectrum due to the slow motion of clutter scatterers, for example, the trees swaying in the wind. The common model of the ground clutter is the Gaussian-shaped power spectrum centered on zero Doppler frequency, as depicted in Fig. 4. It can be seen that the notches of the single canceler are not wide enough to remove most of the clutter spectrum. An improved solution is to use a double canceler.

A *double canceler* is formed by cascading two single cancelers and utilizes three signal pulses, as shown in Fig. 5(a). The frequency response of the double canceler is

$$H(\omega) = [1 - \exp(-j\omega T_r)]^2 = 1 - 2\exp(-j\omega T_r) + \exp(-2j\omega T_r) \tag{17}$$

The magnitude of the frequency response, depicted by the dashed line in Fig. 4, is

$$|H(\omega)| = 4\sin^2(\omega T_r/2) = 4\sin^2(\pi f_D/f_r) \tag{18}$$

Compared with the single canceler, the double canceler provides a broader rejection notch and thus removes more clutter. The second equation of Eq. (17) indicates that the double canceler can be implemented by a transversal filter, or finite impulse response (*FIR*) filter, as shown in Fig. 5(b).

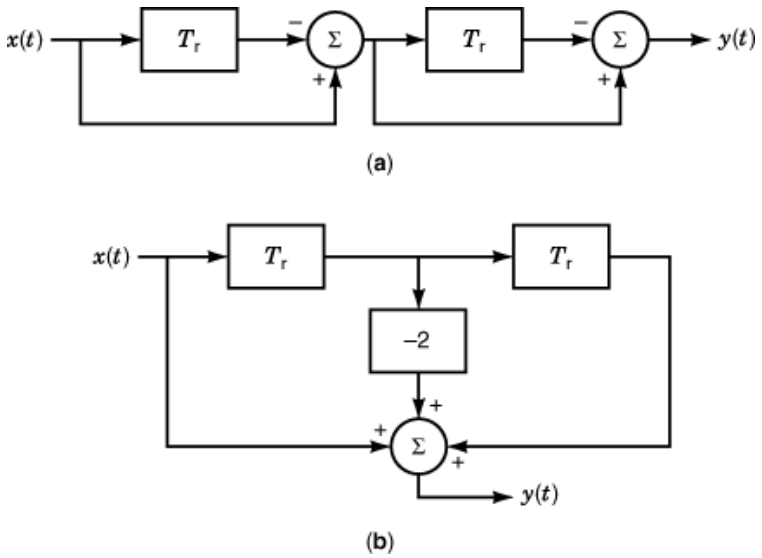


**Fig. 5.** (a) Double canceler is constructed by cascading by two single cancelers. An equivalent implementation is shown in (b), which is a transversal filter, or *FIR* filter.

It is also possible to construct a triple or multiple canceler using similar methods. One advantage of the delay-line canceler is that it is able to process all target and clutter echoes, regardless of range.

**Performance of Moving-Target Indicator.** Many indicators have been used to describe *MTI* performance. Among them, the *MTI* improvement factor is the most widely used. Other indicators used are clutter attenuation, *MTI* gain, subclutter visibility, cancellation ratio, and clutter visibility ratio.

*MTI Improvement Factor.* It is defined 2 as "the signal-to-clutter ratio at the output $(s_o/c_o)$ of the clutter filter divided by the signal-to-clutter ratio at the input $(s_i/c_i)$ of the clutter filter, averaged uniformly over all target radial velocities of interest". The improvement factor accounts for both clutter attenuation and target gain. It can be expressed mathematically as

$$I = \overline{\left(\frac{s_o/c_o}{s_i/c_i}\right)} \tag{19}$$

For the clutter with a zero-mean Gaussian-shaped spectrum, the improvement factors of the single canceler and the double canceler are given, respectively, as (3)

$$I_1 \approx 2(f_r/2\pi\sigma_c)^2 \tag{20}$$

$$I_2 \approx 2(f_r/2\pi\sigma_c)^4 \tag{21}$$

where $\sigma_c$ is the standard deviation of the clutter power spectrum.

*Clutter Attenuation.* The ratio of clutter power at the input of the *MTI* to the power of residual clutter at the output.

*MTI Gain.* The ratio of signal power at the output of the *MTI* to signal power at the input, averaged over all target radial velocities of interest.

From the definitions of the improvement factor, the clutter attenuation, and the *MTI* gain, the relationship between them can be expressed by

$$I = \overline{\left(\frac{s_o/c_o}{s_i/c_i}\right)} = \overline{\left(\frac{s_o}{s_i}\right)}\frac{c_i}{c_o} = G\,\mathrm{CA} \qquad (22)$$

where $G$ is the *MTI* gain and CA is the clutter attenuation.

*Subclutter Visibility.* It is defined (2) as the ratio by which the target echo power may be weaker than the coincident clutter echo power and still be detected with specified detection and false-alarm probabilities. Target and clutter powers are measured on a single pulse return, and all target radial velocities are assumed equally likely. Subclutter visibility measures the capability of the *MTI* to detect moving target in the presence of clutter. For example, 20 dB of subclutter visibility means that the moving target can be detected even though the clutter echo power is 100 times the target echo power.

**Other Moving-Target Indicators.**

*Blind Speed and Staggered-PRF MTI.* As shown in Fig. 4, the frequency responses of the single and double canceler have periodic nulls at multiples of *PRF* $f_r$. If the moving target produces a Doppler frequency that exactly equals $f_r$, or multiples of $f_r$, its echo will also be canceled by the MTI. In other words, radar is not able to detect a target moving at one of these radial velocities. So such a speed is named a blind speed.

Blind speed is actually an inherent phenomenon of pulsed radars in which a sinusoidal signal with the Doppler frequency $f_D$ is discretely sampled at the frequency $f_r$. In the case that $f_D = n f_r$, the sampling occurs at the same point in each corresponding Doppler cycle. Then the moving target looks as if it is stationary.

The problem of blind speed can be alleviated by staggering the *PRF*, because a speed that is blind at one *PRF* is generally not blind at another *PRF*. In this case, the interpulse period of the transmitted signal is changed from pulse to pulse. Time delay in the *MTI* canceler is also changed correspondingly. This type of *MTI* is called staggered-PRF MTI. It has a much higher first blind speed than that of the conventional MTI.

In staggered-PRF MTI, the ratio of interpulse periods is usually expressed by a set of prime integers, which has no common divisor other than 1. If $N$ interpulse periods are staggered by $d_1$: $d_2$: . . . : $d_N$, the increase of the first blind speed $V$ can be expressed by

$$\frac{V}{V_B} = \frac{d_1 + d_2 + \cdots + d_N}{N} \qquad (23)$$

where $V_B$ is the blind speed corresponding to the average interpulse periods.

*Moving-Target Detector.* The moving-target detector (*MTD*) is an enhanced version of traditional MTI. The basic structure of a *MTD* is a *MTI* precanceler followed by a Doppler filter bank. The Doppler filter bank performs the Doppler filtering or Doppler-frequency analysis and is typically implemented by the fast Fourier transform (*FFT*). A Doppler filter bank using $N$ -pulse *FFT* divides the whole frequency band into $N$ parts, which are processed separately.

The Doppler filter bank provides the following advantages: (1) The *SNR* is improved since the signal in a certain filter only competes with interference that can pass the filter. (2) The Doppler frequency of a target can be measured to a high accuracy. (3) Moving clutter with a nonzero mean of Doppler shift can be rejected by separately adjusting the threshold of each filter. (4) A clutter map can be generated using the output from the filter banks.

*Adaptive MTI.* The adaptive *MTI* is able to adaptively shift its rejection notch to the location of the clutter spectrum. It is very useful for canceling moving clutter, whose Doppler frequency is not zero. An example of adaptive *MTI* implementation is the time-averaged-clutter coherent airborne radar (*TACCAR*) (4). A phase-error circuit estimates the phase change of clutter signals between pulses, which is caused by its

Doppler frequency. The averaged estimate of phase error is used to control the coherent oscillator (*COHO*) to produce a phase-shifted reference signal for mixing with the return signal. This is equivalent to shifting the Doppler center of the moving clutter to zero. Then a conventional *MTI* can be used to cancel the clutter. Other implementation methods of adaptive *MTI* includes changing the weights of the *MTI* filter and using modern spectral estimation method.

*Airborne MTI.* The airborne *MTI* (AMTI) refers to the *MTI* techniques utilized by a moving radar. The relative motion between radar and fixed clutter displaces the Doppler spectrum of clutter from zero. Thus, the adaptive *MTI* is one of the AMTI techniques. Another adverse effect of platform motion is the loss of signal correlation between adjacent pulses, because the illuminated area is slightly displaced from one pulse to the next. The effects of platform motion can be mitigated by physically or electrically displacing the antenna phase center along the plane of the aperture. This technique is called displaced phase center antenna (*DPCA*).

A relatively new technique is named space-time adaptive processing (*STAP*). It simultaneously cancels clutter in angle (space) and Doppler (time) domain. For example, the clutter coming from the antenna mainlobe is spread out in Doppler frequency due to platform motion and is not easy to be canceled in the Doppler domain. The *STAP* technique can effectively resolve the clutter within the beam width into angle Doppler cells. Targets can be detected in cells that are not occupied by clutter.

## Beam Forming

The radar often encounters jamming interference in military environment. The jamming source usually occupies the same frequency band as the desired signal and is difficult to eliminate by frequency filtering. Fortunately, the spatial location of jamming source is usually different from that of the target. Spatial filtering can thus be used to separate them in the space domain.

Spatial filtering in radar is achieved by forming a specific radar antenna beam pattern. A narrow mainlobe means good selectivity, and low sidelobes means strong rejection capability. However, producing an antenna with very low sidelobes in all directions is difficult to achieve in practice. High-power interfering signals can still come into the receiver through sidelobes and degrade the desired signal. Furthermore, the direction of jamming source may change with time. The beam-forming technique deals with this problem. It is able to adaptively form an antenna beam pattern with a very low sidelobe in the direction of the interference.

Beam forming utilizes array antennas and only considers signal reception. The array elements are discrete spatial samples over the entire antenna aperture. The signals received by each element are weighted and summed to form the array output. When the weights of array elements can be adaptively adjusted, it is called *adaptive beam forming*.

**Linear Array Model and Classical Beam Forming.** An ideal linear array consists of identical, omnidirectional, equispaced sensors that are located along a straight line. Figure 6 shows a linear array beam former for processing narrowband signals. At time instant $k$, each sensor samples the arriving signal. The output of the beam former is calculated as

$$y(k) = \sum_{n=1}^{N} w_n^* x_n(k) \tag{24}$$

where $x_n(k)$ is the input signal of sensor $n$ at time $k$. For the convenience of notation, a complex conjugate is applied to the weight $w_n$. Equation (24) can be rewritten in the following vector form:

$$y(k) = \boldsymbol{w}^{\mathrm{H}} \boldsymbol{x}(k), \tag{25}$$

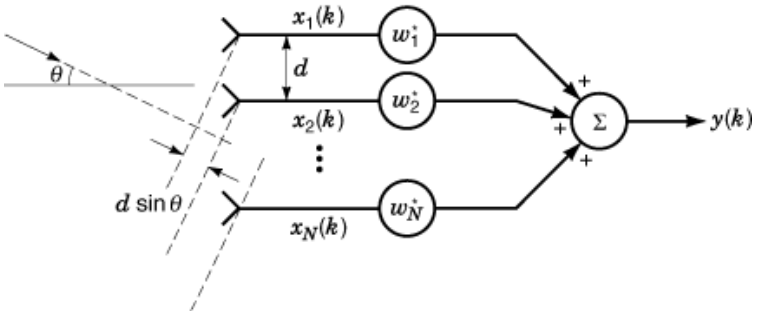


**Fig. 6.** In the linear array model for processing narrowband signals, the signals received by each element are weighted and summed to form the array output.

where $\boldsymbol{w}$ and $\boldsymbol{x}$ are $N$-dimensional column vectors and H denotes the transposed conjugate.

The array receives plane waves from a target if it is located in the far field. Assume that the signal has a carrier frequency $f$ and comes from direction $\theta$, which is defined as the angle of incidence with respect to the broadside of the array. If two adjacent array elements are separated by a distance $d$, the signals they received have a phase difference of

$$\phi(\theta, f) = 2\pi(f/c)d \sin\theta \tag{26}$$

where $c$ is the speed of light. In the following analysis, we assume a fixed carrier frequency $f$. So $\phi(\theta, f)$ is simply denoted by $\phi(\theta)$. At time instant $k$, if the signal received by the first element is $A(k)\exp[j\phi_1(k)]$, that received by the $n$th element is $A(k)\exp\{j[\phi_1(k) - (n-1)\phi(\theta)]\}$.

If the first element is used as reference, which means the phase of its signal, $\phi_1(k)$, is set to zero, then the phase of each array element can be written as

$$d(\theta) = \left(1, \exp[j\phi(\theta)], \ldots, \exp[j(N-1)\phi(\theta)]\right)^{\mathrm{H}} \tag{27}$$

This vector is termed the steering vector, which is also known as the direction vector, array manifold, or array response vector. The output of the beam former can be expressed as

$$y(k) = \boldsymbol{w}^{\mathrm{H}}\boldsymbol{x}(k) = A(k)\boldsymbol{w}^{\mathrm{H}}\boldsymbol{d}(\theta) \tag{28}$$

The normalized output is denoted by

$$\boldsymbol{r}(\theta) = \boldsymbol{w}^{\mathrm{H}}\boldsymbol{d}(\theta), \tag{29}$$

where $r(\theta)$ is called the beam former response. The square of $r(\theta)$ is defined as the beam pattern.

In classical beam forming, the objective is to approximate the ideal response that is unity in a desired direction and zero elsewhere. The classical beam former, also known as the conventional beam former, is used to receive a desired signal coming from a known direction $\theta_0$. The solution is to choose the weight as $\boldsymbol{w} = \boldsymbol{d}(\theta_0)$.

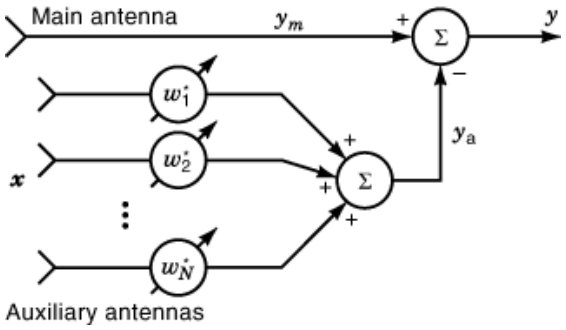


**Fig. 7.** The multiple sidelobe canceler consists of a main antenna and an auxiliary adaptive beam former. The latter estimates the interference in the main channel, which is then subtracted from the main channel.

From Eq. (29) the beam former response is

$$r(\theta) = \sum_{n=0}^{N-1} \exp\{-jn[\phi(\theta) - \phi(\theta_0)]\} = \mathrm{S}_N\{[\phi(\theta) - \phi(\theta_0)]/2\}, \tag{30}$$

where $\mathrm{S}_N(x)$ is defined as

$$\mathrm{S}_N(x) = N\sin(Nx)/(N\sin x) \tag{31}$$

and is called the periodic sinc function. The peak of the response is located at angle $\theta_0$. So the mainlobe of the beam points to $\theta_0$. It is also said that the beam is steered to $\theta_0$. In practice, amplitude tapering or weighting is usually used to control the sidelobe levels. As $r(\theta)$ is the summation of the phase-shifted output of each element, the beam former is also termed *a phased array*.

### Adaptive Beam Forming.

*Multiple Sidelobe Canceler.* As stated earlier, strong jamming sources usually come into the receiver through antenna sidelobes. It is thus desirable to form a beam pattern with nulls in the directions of the jamming sources. The multiple sidelobe canceler (MSC) is the earliest beam former that achieves this goal. An MSC consists of a main antenna and one or more auxiliary antennas, as shown in Fig. 7. The mainlobe of the main antenna points to the target of interest. Interfering signals are assumed to enter through its sidelobes. It is assumed that the auxiliary antennas only receive interfering signals and noise. The weight of each element can be adaptively adjusted to produce an output that estimates the interfering signals in the main channel. Subtracting the output from the main channel by this estimate effectively cancels the interference in the main channel.

Denote the signal in the main channel by $y_m$, the input of auxiliary antennas by $\boldsymbol{x}_\mathrm{a}$, and the weight vector by $\boldsymbol{w}$. The output of the auxiliary array is $y_\mathrm{a} = \boldsymbol{w}^\mathrm{H}\,\boldsymbol{x}_\mathrm{a}$. Since $y_\mathrm{a}$ is assumed not to contain the target signal, successful cancellation of interference is equivalent to minimization the overall output power $\boldsymbol{E}[|y_\mathrm{m} - y_\mathrm{a}|^2]$, that is,

$$P_{\min} = \min_w E\left(|\, y_m - \boldsymbol{w}^\mathrm{H}\boldsymbol{x}_a\,|^2\right) \tag{32}$$

The weight that satisfies the above equation is called the optimum weight, which is given by (5)

$$\boldsymbol{w}_{\text{opt}} = \boldsymbol{R}_{\text{a}}^{-1}\boldsymbol{p}_{\text{am}} \tag{33}$$

where $\boldsymbol{R}_{\text{a}} = E[\boldsymbol{x}_{\text{a}}\,\boldsymbol{x}^{\text{H}}{}_{\text{a}}]$ is the covariance matrix of input data in auxiliary antennas, and $\boldsymbol{p}_{\text{am}} = E[\boldsymbol{x}_{\text{a}}\,y^{*}{}_{\text{m}}]$ is the cross-correlation vector of $\boldsymbol{x}_{\text{a}}$ and $y_m$ .

One should notice the assumption that the target signal is absent in the auxiliary antennas. This is necessary. Otherwise, it will cause cancellation of target signal in the final output. However, the MSC can still work well with slight signal loss if the target signal in the auxiliary antennas is very small.

*Linearly Constrained Adaptive Beam Forming.* Another popular class of adaptive beam-forming techniques is the linearly constrained adaptive beam forming. It prevents the loss of desired signal by imposing linear constraints on the weights. Equation (29) shows that the beam-former response to a signal from direction $\theta$ is $\boldsymbol{w}^{\text{H}}\,\boldsymbol{d}(\theta)$. If the direction of interest is $\theta_0$, the constraint can be expressed as $\boldsymbol{w}^{\text{H}}\,\boldsymbol{d}(\theta_0) = f$, where $f$ is constant. It ensures that the desired signal from angle $\theta_0$ will pass the beam former with response $f$. Thus, minimizing the overall output power, $E[|y|^2] = \boldsymbol{w}^{\text{H}}\,\boldsymbol{R}_{\text{x}}\,\boldsymbol{w}$, will minimize the output produced by interference and noise from directions other than $\theta_0$. The linearly constrained beamforming can be expressed as

$$\min_{\boldsymbol{w}} \boldsymbol{w}^{H}\boldsymbol{R}_{\text{x}}\boldsymbol{w} \quad \text{subject to} \quad \boldsymbol{w}^{\text{H}}\boldsymbol{d}(\theta_0) = f \tag{34}$$

The solution of the optimum weight is

$$\boldsymbol{w} = f^{*}\frac{\boldsymbol{R}_{\text{x}}^{-1}\boldsymbol{d}(\theta_0)}{\boldsymbol{d}^{H}(\theta_0)\boldsymbol{R}_{x}^{-1}\boldsymbol{d}(\theta_0)} \tag{35}$$

When $f = 1$, the beam former is also termed the minimum variance distortionless response (*MVDR*) beam former. There is only one constraint on $\boldsymbol{w}$ in Eq. (34). In fact, multiple constraints can also be used to add more control on the beam former response (6).

The generalized sidelobe canceler (*GSC*) (7) is an alternative approach to the linearly constrained adaptive beam forming. It converts the constrained optimization of Eq. (34) to unconstrained optimization by separating out the constraint. Figure 8 shows the structure of the *GSC*. The upper or main branch is a classical beam former, which has a fixed weight $\boldsymbol{w}_c$. The weight $\boldsymbol{w}_c$ is chosen so that the response of the main beam former satisfies the constraint in Eq. (34). So the desired signal from angle $\theta_0$ will pass the main beam former with desired response $f$. Interference and noise will produce some output determined by $\boldsymbol{w}_c$. The lower branch is an adaptive beam former, which is used to estimate the output produced by interference and noise in the main beam former. The estimate is then subtracted from the main branch to cancel the interference and noise in the final output. This is similar to that in the MSC. The difference is that there is a preprocessing matrix $\boldsymbol{B}$ in the lower branch of the *GSC*. The purpose of $\boldsymbol{B}$ is to block the desired signal and thus to prevent signal cancellation in the final output. So $\boldsymbol{B}$ is named the blocking matrix. For an array that is not presteered, $\boldsymbol{B}$ needs to satisfy $\boldsymbol{d}^{\text{H}}(\theta_0)\boldsymbol{B} = 0$. The columns of $\boldsymbol{B}$ are linearly independent, and the number of columns $L$ should be less than the number of array elements.

The overall output of the *GSC* is $y = y_m - y_a$, where $y_m$ and $y_a$ are the output of the upper and lower beam formers, respectively. Since $y_a$ does not contain the desired signal, cancellation of interference and noise is again equivalent to minimize the overall output power

$$\min_{\boldsymbol{w}_a} E[\,|y_m - y_a|^2] \tag{36}$$

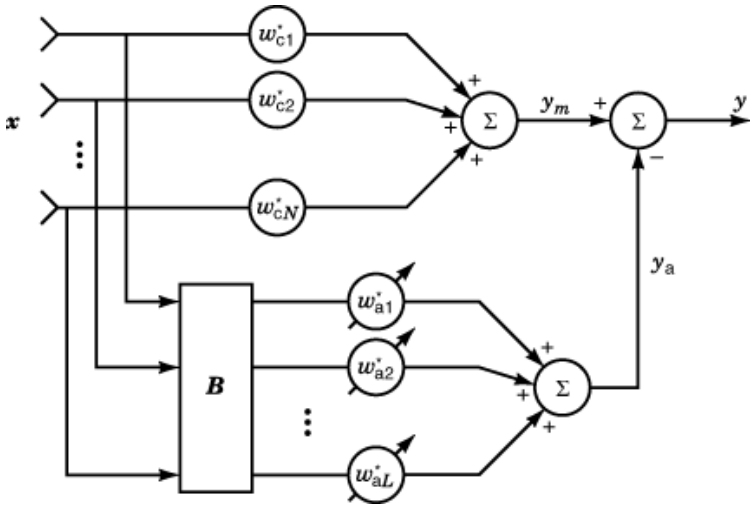


**Fig. 8.** The upper channel of the generalized sidelobe canceler is a classical beam former, which has a constant response to the desired signal. The lower channel is an adaptive beam former. It estimates the interference in the upper chanel, which is then subtracted from the upper channel. The blocking matrix $B$ blocks desired signal and thus prevent signal cancellation.

The solution to the unconstrained optimization is

$$\boldsymbol{w}_a = (\boldsymbol{B}^{\mathrm{H}}\boldsymbol{R}_{\mathrm{x}}\boldsymbol{B})^{-1}\boldsymbol{B}^{\mathrm{H}}\boldsymbol{R}_{\mathrm{x}}\boldsymbol{w}_{\mathrm{c}}, \tag{37}$$

where $\boldsymbol{R}_{\mathrm{x}} = E[\boldsymbol{x}\boldsymbol{x}^{\mathrm{H}}]$ is the covariance matrix of input data.

Besides the MSC and the *GSC*, there are some other criteria for constructing an adaptive beam former, such as using a reference signal or maximizing the *SNR*.

*Adaptive Algorithms.* Calculation of the optimum weights for the adaptive beam formers discussed before requires the knowledge of second-order statistics, especially the covariance of the input signal. Such information is normally not available and needs to be estimated from received data. The optimum weights are usually estimated and adjusted by adaptive algorithms.

It can be proved that the adaptive beam-forming problem is equivalent to the adaptive filtering. So the many adaptive algorithms developed for adaptive filtering can be utilized for adaptive beam forming. One popular class of adaptive algorithms is based on the gradient, for example, the widely used least-mean-square (*LMS*) algorithm. Another important class is based on the least-square estimation, such as the sample matrix inversion (*SMI*) and the recursive least square (RLS) algorithm. There is a separate article in this encyclopedia, Radar signal detection that discusses the adaptive filtering technique. For details of these adaptive algorithms, please refer to that article.

## Constant False-Alarm Rate

A radar detector makes decision of target presence or absence from the echo of each resolution cell. If the echo is stronger than a prespecified threshold, the decision of target presence is made. Otherwise, it declares no target. The basic parameters of a radar detector are the probability of false alarm and the probability of detection. The article Radar signal detection in this encyclopedia discusses basic theories of radar detection.

This article focuses on an advanced technique for the detector to maintain approximately constant false-alarm rate (*CFAR*).

**CFAR Principles.** We first investigate the principles of CFAR in the background of Gaussian interference. In this case, the interfering signals in both channels of I and Q, denoted by $x$ and $y$ respectively, are Gaussian processes with zero mean and variance (power) of $\sigma^2$. This is a common model for noise and many types of clutter. A linear envelope detector produces the signal envelope or magnitude, $r = \sqrt{x^2 + y^2}$, which is used for target detection. The $r$ has a Rayleigh probability density function (*PDF*) as

$$p(r) = \frac{r}{\sigma^2} \exp\left(-\frac{r^2}{2\sigma^2}\right) \tag{38}$$

The mean value of $r$ is

$$E[r] = \sigma\sqrt{\pi/2} \tag{39}$$

The false-alarm probability $P_{\mathrm{FA}}$ for a given threshold $r_{\mathrm{t}}$ can be calculated as

$$P_{\mathrm{FA}} = \int_{r_t}^{\infty} p(r)dr = \exp(-r_t^2/2\sigma^2) \tag{40}$$

The $P_{\mathrm{FA}}$ is extremely sensitive to the changes of interference power $\sigma^2$. For example, doubling the interference power can increase the value of $P_{\mathrm{FA}}$ from $10^{-8}$ to $10^{-4}$. Hence, it is necessary to maintain approximately constant false-alarm rate in order to ensure that the radar works well when the intensity of interference changes. This can be achieved by adaptively adjusting the threshold according to the interference power. An equivalent method is to normalize the interference signal so that its *PDF* will be independent of its power $\sigma^2$.

Normalization of the Gaussian processes $x$ and $y$ is done by computing $x/\sigma$ and $y/\sigma$. Correspondingly, the normalized envelope is

$$r_{\mathrm{N}} = \sqrt{(x/\sigma)^2 + (y/\sigma)^2} = r/\sigma \tag{41}$$

Its *PDF* becomes

$$p(r_{\mathrm{N}}) = p(r = \sigma r_{\mathrm{N}})/|dr_{\mathrm{N}}/dr| = r_{\mathrm{N}} \exp(-r_{\mathrm{N}}^2/2) \tag{42}$$

The false-alarm probability is

$$P_{\mathrm{FA}} = \int_{r_t}^{\infty} p(r_{\mathrm{N}})dr_{\mathrm{N}} = \exp(-r_t^2/2) \tag{43}$$

It can be seen that the new false-alarm probability is independent of the interference power $\sigma^2$. This is the desired property of CFAR. Therefore, if $\sigma$ can be estimated from the received signals, the normalization process $r/\sigma$ will produce the constant false-alarm rate. From Eq. (39), we know that an estimate of $\sigma$ can be obtained by estimating the mean value of $r$.

An alternative method is to use a square-law envelope detector. The magnitude squared of the envelope is produced, denoted by $q = r^2$, and used for deciding the presence of the target. The *PDF* of $q$ can be calculated

from Eq. (38) as

$$p(q) = p(r = \sqrt{q})/|dq/dr| = \frac{1}{2\sigma^2}\exp\left(\frac{-q}{2\sigma^2}\right) \qquad (44)$$

The mean value of $q$ is

$$E[q] = 2\sigma^2 \qquad (45)$$

Normalization of $q$ can be done as

$$q_N = r_N^2 = r^2/\sigma^2 = q/\sigma^2 \qquad (46)$$

The *PDF* of the normalized variable $q_N$ is

$$p(q_N) = p(q = \sigma^2 q_N)/|dq_N/dq| = \exp(-q_N/2)/2 \qquad (47)$$

In this case, the false-alarm probability for a preset threshold $q_t$ is

$$P_{FA} = \int_{q_t}^{\infty} p(q_N)dq_N = \exp(-q_t/2) \qquad (48)$$

The false-alarm probability is independent of $\sigma^2$. So the CFAR property is achieved by the normalization of $q/\sigma^2$. Equation (45) indicates that an estimate of $\sigma^2$ can be obtained by estimating the mean value of $q$ .

The CFAR principle in the presence of Gaussian interference has been discussed for the linear and square-law envelope detectors. For non-Gaussian interference, its envelope cannot be represented by the Rayleigh *PDF* model. Specific models, such as the log-normal or the Weibull distribution must be used according to the environment and application. In such cases, the CFAR can still be achieved by proper normalization of the interference signal. The CFAR processing protects the radar detector from excessive numbers of false alarms. The cost is that the probability of detection will be slightly reduced compared with similar cases of thermal-noise-only environment.

**Cell-Averaging CFAR.** As analyzed before, for Gaussian interference, the normalization factor can be obtained by estimating the mean value of the signal output from the envelope detector. One basic approach of CFAR is to estimate the mean value by averaging the signals of a set of reference cells around the cell under test. This technique is called cell-averaging CFAR (CA-CFAR). The reference cells can be either in range, angle, or Doppler frequency. The basic assumption in CA-CFAR is that the interference is statistically homogeneous over the reference cells and the cell under test.

Figure 9 shows the structure of the CA-CFAR processor that uses reference cells in range. The envelope detector can have either a linear characteristic that produces the envelope $r$ or a square-law characteristic that produces the magnitude squared of envelope $q$. The received signals from the reference cells are averaged to produce an estimate of their mean value. The immediate neighbors of the test cell are sometimes discarded in case a strong target signal extended into them. The signal of the test cell is then normalized by dividing it by the estimated mean and multiplying it with a scaling constant $k$. We know from Eqs. (39) and (45) that $k = \sqrt{\pi/2}$ for the linear detector and $k = 2$ for the square-law detector. Finally the normalized envelope of the test cell is compared with a preset threshold to decide if a target is present.

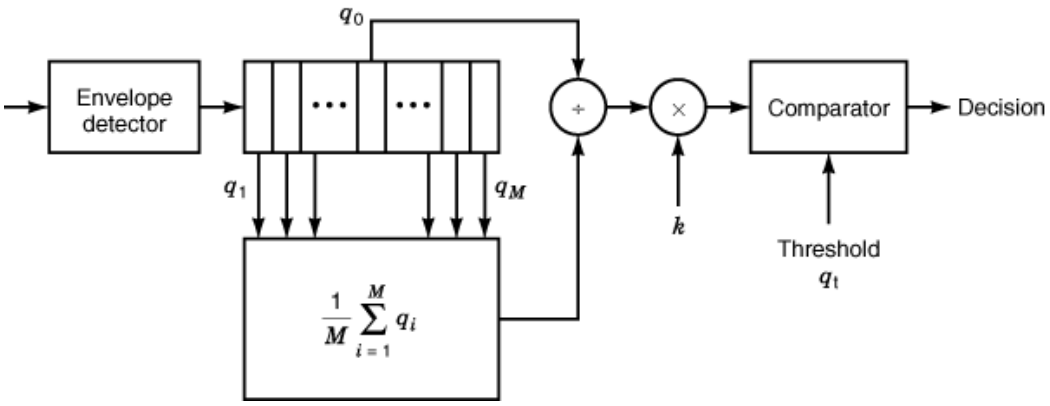


**Fig. 9.** A number of reference cells around the cell under test are used to estimate the interference power in the cell-averaging CFAR processor. The estimate is used to normalize the signal, which is equivalent to adaptively adjusting the threshold.

The CA-CFAR principle is applicable to both linear and square-law detection. The analysis that follows is developed for square-law detection without loss of generality. Denote the magnitude squared of envelope of the test cell by $q_0$, and that of the reference cells by $q_i (i = 1, \ldots, M)$. These random variables are statistically independent and have the same probability density function in a homogeneous environment as given in Eq. (44). Their joint density function is

$$p(q_0, \ldots, q_M) = \prod_{i=0}^{M} \frac{1}{2\sigma^2} \exp\left(\frac{-q_i}{2\sigma^2}\right) \tag{49}$$

Denote the sum of the $M$ reference cells by $q_M = \Sigma q_i$. The normalization of $q_0$ is

$$q_{0N} = kMq_0/q_M = 2Mq_0/q_M \tag{50}$$

$q_{0N}$ is then compared with a threshold $q_t$, and the target-present decision is made when

$$q_{0N} > q_t \tag{51}$$

In practice, only a limited number of reference cells $M$ can be utilized to estimate the mean value. Intuitively, the performance of CA-CFAR must be dependent on $M$. Substituting Eq. (50) into Eq. (51), we get

$$q_0/q_M > q_t/(2M) \tag{52}$$

For random variables $q_i (i = 1, \ldots, M)$ having the density function given by Eq. (49), the ratio $q_0/q_M$, called $f$ variate, is known to have the following *PDF* (8):

$$p(f) = M/(1+f)^{M+1}, \qquad 0 \le f < \infty \tag{53}$$

The false-alarm probability can then be calculated as

$$p_{\mathrm{FA}} = \int_{q_\mathrm{t}/2M}^{\infty} p(f)df = \left(1 + \frac{q_\mathrm{t}}{2M}\right)^{-M} \tag{54}$$

It can be seen from Eq. (54) that the CFAR property can be achieved even for small values of $M$, since the false-alarm probability is independent of the interference power $\sigma^2$. Equation (54) approximates the ideal performance when $M$ is very large such that

$$\lim_{M\to\infty}\left(1 + \frac{q_\mathrm{t}}{2M}\right)^{-M} = \exp(-q_\mathrm{t}/2) \tag{55}$$

For a limited number of reference cells, higher signal-to-noise ratio is needed to achieve the required false-alarm probability and detection probability. This is referred to as the CFAR loss.

For Swerling I and II targets, one can find the detection probability using similar methods. The signals of a Swerling I or II target in I and Q channels are also modeled as a zero-mean Gaussian process with a variance of ${\sigma^2}_\mathrm{s}$. The overall variance is thus ${\sigma^2}_\mathrm{s} + \sigma^2$ when the target is present. Denote the signal-to-noise ratio by SNR $= {\sigma^2}_\mathrm{s}/\sigma^2$. A similar analysis shows the detection probability $P_\mathrm{d}$ is

$$P_\mathrm{d} = \left(1 + \frac{q_\mathrm{t}}{2M(1+\mathrm{SNR})}\right)^{-M} \tag{56}$$

and

$$\lim_{M\to\infty} P_\mathrm{d} = \exp\left(-\frac{q_\mathrm{t}}{2(1+\mathrm{SNR})}\right) \tag{57}$$

For given $P_{\mathrm{FA}}$ and $P_\mathrm{d}$, the *SNR* for $M$ reference cells, denoted by $\mathrm{SNR}_M$, can be derived from Eqs. (54) and (56). On the other hand, the *SNR* for $M \to \infty$, denoted by $\mathrm{SNR}_\infty$, can be obtained from Eqs. (55) and (57). The CFAR loss is defined as the ratio of $\mathrm{SNR}_M$ and $\mathrm{SNR}_\infty$. It is a function of $P_{\mathrm{FA}}$, $P_\mathrm{d}$, and $M$. It has been shown (9) that for large $M$, the CFAR loss can be approximated by ${P^{-1/2\mathrm{M}}}_{\mathbf{FA}}$.

**Ordered-Statistics CFAR.** The CA-CFAR does not work well for nonhomogeneous interference. One example is when there are interfering targets in the reference cells. Another case is when the background clutter varies dramatically along either range or azimuth or both. Cell averaging can no longer produce the correct estimate, which results in the loss of detection performance. The ordered-statistics CFAR (OS-CFAR) has been proven to have better performance in such environments.

In the OS-CFAR, the threshold is determined by multiplying one of the ranked cell by a scaling factor. Assume that the reference cells have the signals of $q_\mathrm{i}(i = 1, \ldots, M)$ after the envelope detector. They are ranked as $q_1 \le q_2 \le \cdots \le q_\mathrm{K} \le \cdots \le q_\mathrm{M}$. The variable $K$ is the rank of the cell to be used for calculating the threshold, which is

$$q_\mathrm{t} = \alpha q_K \tag{58}$$

The scaling factor $\alpha$ provides a mechanism to control the false-alarm probability.

**Clutter-Map CFAR.** The clutter-map CFAR is an effective approach for dealing with nonhomogeneous interference. It utilizes the statistics of past observations on the test cell itself rather than that of the reference cells. It assumes that the statistics of the test cell do not change during the observations so that time averaging can be performed. In fact, the average of previous observations on each cell produces a clutter map—an estimate of clutter power in each corresponding cell.

The principle of clutter-map CFAR is similar to that of the CA-CFAR. The basic analysis of CA-CFAR is applicable to clutter-map CFAR. In clutter-map CFAR processing, the $M$ reference samples are obtained from $M$ scans on the test cell. They are averaged in the same way as that in CA-CFAR to produce an estimate of the interference power. Further processing is also similar to CA-CFAR. In a new scan, if the target-present decision is made, the power estimate will not be updated. Otherwise, the new sample is used to compute a new average.

A simplified implementation is to store only the estimate by previous samples, denoted by $\hat{p}_{n-1}$ from previous $n-1$ scans, and updates the estimate with the new sample $q_n$:

$$\hat{p_n} = (1-w)\hat{p}_{n-1} + wq_n \tag{59}$$

This is actually an exponential smoothing, since

$$\hat{p_n} = w\sum_{i=0}^{\infty}(1-w)^i q_{n-i} \tag{60}$$

The value of $w$ determines the length of the exponential window. In practice, the length of the window should be chosen to commensurate with the rate of change of the interference power.

## Pulse Compression

Pulse compression is a technique that obtains high range resolution while maintaining good detection range. Signals used for pulse compression should have large bandwidth. There are two approaches to increase the bandwidth: frequency modulation (*FM*) and phase coding. The device that performs the pulse compression is the matched filter.

**Frequency Modulation Waveforms.** The linear *FM* signal is the earliest pulse compression waveform. Techniques for linear *FM* pulse compression are well developed and widely used. Another relatively new technique adopts the stepped-frequency waveforms.

*Principles of Linear FM Pulse Compression.* The linear *FM* signal, whose carrier frequency varies linearly during the pulse, is the most widely used waveform. It is also known as the *chirp* signal and can be expressed by

$$s_i(t) = A\cos(2\pi f_0 t + \pi\mu t^2), \qquad -T/2 \le t \le T/2 \tag{61}$$

where $f_0$ is the carrier frequency. The constant $\mu$ is called the chirp rate. The instantaneous frequency of the signal is $f_i = f_0 + \mu\, t$, which starts at $f_0 - \mu\, t/2$ and ends at $f_0 + \mu\, t/2$. The signal bandwidth is $B = \mu\, t$ .

It can be shown (10) that the matched filter for the linear *FM* pulse compression can be expressed as

$$h(t) = \sqrt{j\mu}\exp[j2\pi(f_0 t - \mu t^2/2)] \tag{62}$$

The $h(t)$ has an inverse chirp rate as compared with the input signal. The output of the matched filter is

$$\begin{aligned} s_0(t) &= \int_{-\infty}^{\infty} s_i(\tau) h(t-\tau)\, d\tau \\ &= \sqrt{j\mu} \int_{-T/2}^{T/2} \exp\{j2\pi[f_0\tau \\ &\quad + \mu\tau^2/2 + f_0(t-\tau) - \mu(t-\tau)^2/2]\}\, d\tau \\ &= \sqrt{j\mu T^2}\, \frac{\sin(\pi\mu T t)}{\pi\mu T t} \exp[j2\pi(f_0 t - \mu t^2/2)] \end{aligned} \quad (63)$$

The envelope of the output signal is a sinc function

$$e_0(t) = \sqrt{\mu T^2}\, \frac{\sin(\pi\mu T t)}{\pi\mu T t} \quad (64)$$

For the sinc function, the peak-null pulse width is defined as the distance from the peak to the first null. For sin $x/x$, the first null occurs at $x = \pi$. So the width of the compressed pulse is

$$T' = \frac{1}{\mu T} = \frac{1}{B} \quad (65)$$

It equals the reciprocal of the signal bandwidth. The pulse compression ratio is defined as the ratio of the pulse width before and after the pulse compression processing. From Eq. (65), we have

$$D = T/T' = TB \quad (66)$$

Therefore, the pulse compression ratio is equal to the time–bandwidth product of the signal.

From Eq. (3), the range resolution after pulse compression is

$$\rho_r = \frac{cT'}{2} = \frac{c}{2B} \quad (67)$$

It should be noted that the peak-null pulse width corresponds to the mainlobe width at $-4$ dB (power) points. Another definition of pulse width is the mainlobe width at $-3$ dB, which is called half-power pulse width and can be expressed as $K_w/B$, where $K_w$ is a constant factor. For the sinc function, $K_w = 0.866$.

It is well known that the sinc function has high sidelobes. To reduce sidelobes, one approach is to apply weighting in the compression filter. It can greatly reduce the sidelobes at the cost of mainlobe broadening. Table 1 lists some popular weighting functions with the corresponding peak sidelobe levels and mainlobe width at $-3$ dB. Another approach to reduce the sidelobes is to use nonlinear *FM* waveforms. In this case, the spectrum of the transmitted signal is weighted, which also provides low sidelobes in the compressed pulse.

*Implementation of Linear FM Pulse Compression.* The commonly used analog devices for linear *FM* pulse compression are the dispersive delay lines, in which the signal delay is dependent on its frequency. The most popular one is the surface acoustic wave (*SAW*) device. The electrical signal is converted into a surface wave at the input, which propagates through the medium at acoustic speed. The dispersive property of the device achieves the matched filtering. At the output the wave is converted back to the electrical signal. Another

**Table 1. Properties of Weighting Functions**

| Weighting Function | Peak Sidelobe Level (dB) | Mainlobe Width at −3 dB, $K_w/B$ |
|---|---|---|
| Rectangular | −13.26 | 0.886/$B$ |
| Hanning | −31.5 | 1.42/$B$ |
| Hamming | −42.5 | 1.32/$B$ |
| Taylor, $\bar{n} = 5$ | −35 | 1.19/$B$ |
| Taylor, $\bar{n} = 6$ | −40 | 1.25/$B$ |
| Dolph–Chebyshev | −40 | 1.20/$B$ |

type of ultrasonic device is called bulk acoustic wave device, which is less energy efficient than the *SAW* device. These ultrasonic devices can process signals with bandwidth greater than 1000 MHz (10).

Linear *FM* pulse compression can also be implemented by digital methods. The received signal is sampled by an *ADC* and transformed into the frequency domain via *FFT*. The matched filtering is performed in the frequency domain by multiplying the signal spectrum with the frequency response of the matched filter. The result is then transformed back into the time domain.

A third technique is called stretch processing, which can process signals with very large time–bandwidth products. Figure 1 shows its principle. Echoes from a set of scatterers are linear *FM* signals whose starting points correspond to the ranges of each scatterer. They are mixed with a reference signal, which is also a linear *FM* with the same chirp rate as that of the transmitted signal. The mixing (dechirping) process removes the frequency modulation of the received signal. Each dechirped signal has a constant frequency that corresponds to its range. An *ADC* then samples these dechirped signals. Finally, a frequency analysis by *FFT* distinguishes each scatterer in range. The stretch processing is also widely used in high-resolution radars.

*Stepped-Frequency Waveforms.* In this pulse compression technique, the radar transmits a burst of narrowband pulses, and the carrier frequency changes discretely from pulse to pulse by a step size $\Delta f$. Compared with the linear *FM* waveform, the stepped-frequency waveforms can be regarded as discrete modulation in frequency. If there are $N$ pulses in a burst, the overall bandwidth of the transmitted signal is $B = N\Delta f$ .

Each received pulse is then down-converted to baseband, and a pair of I and Q samples is collected in a desired range gate. The length of the range gate is determined by $\Delta f$, which is $r = c/(2\Delta f)$. The ensemble of I and Q samples represent results that the received signal within the desired range gate is discretely sampled in the frequency domain over the bandwidth $B$. There is a condition to be satisfied. That is, the duration of the baseband response of each pulse should extend the whole desired range gate. This is ensured if $T_p \geq 1/\Delta f$, where $T_p$ is the duration of each pulse.

Pulse compression is accomplished by applying the inverse discrete Fourier transform on the $N$ pairs of I and Q samples. The result is a high-resolution range profile with $N$ complex samples over the desired range gate. The length of the range profile is $r$, and the resolution is

$$\rho_r = \frac{c}{2B} = \frac{c}{2N\Delta f} \tag{68}$$

Pulse compression using the stepped frequency avoids the requirements of wide instantaneous bandwidth and high sampling rates. However, transmitting multiple pulses require relatively long time. When there is large motion between the radar and the target, the motion-induced phase errors between pulses must be compensated before the pulse compression can be performed.

**Phase-Coded Waveforms.** The phase-coded signal is a constant-amplitude sinusoid that is divided into $N$ equal segments. The phase of the sine wave in each segment is selected according to a given code

sequence. If the phase is set at either 0 or $\pi$, it is called binary, or biphase, coding. If the code sequence contains more than two values, it is called polyphase coding.

The pulse compression principle can be demonstrated by correlation processing, which is equivalent to matched filtering. Consider a binary-coded signal with $N$ segments. Denote the value of the $k$th segment by $a_k$, which is either 1 or $-1$. The aperiodic autocorrelation function of this waveform can be written as

$$\Phi(m) = \sum_{k=1}^{N} a_k a_{k+m}, \qquad -(N-1) \le m \le N-1 \qquad (69)$$

If $m = 0$, then $a_k\ a_{k+m} = 1$ for each segment $k$, and the summation equals $N$. When $m \neq 0$, the value of the autocorrelation function is much smaller than $N$. Thus the correlation processing produces a narrow pulse, whose mainlobe locates at $m = 0$ with the amplitude of $N$. The regions where $m \neq 0$ are sidelobes. A well-designed code sequence can produce a pulse with very low sidelobes.

The Barker codes are the binary codes that have the lowest peak sidelobe. The aperiodic autocorrelation of Barker codes has the value of either 0 or 1 for $m \neq 0$, and hence the peak sidelobe is 1. With respect to the mainlobe, the peak sidelobe level is $\frac{1}{13}$, or $-22.3$ dB. However, no Barker codes whose length is greater than 13 have been found. The pulse compression ratio for Barker codes is limited to the maximum value of 13. So it is important to find longer sequences with good sidelobe properties.

The minimum peak sidelobe codes are the binary sequences that attain the lowest peak sidelobes for a given length. Of course, the Barker codes belong to this class of codes. Codes with length of 14 to 48 have been found (11). For example, for length 48, the best peak sidelobe that can be achieved is 3, which is $-24.1$ dB with respect to the mainlobe. Other types of long binary codes are random and pseudorandom codes, in which the phase value of 0 or $\pi$ are chosen in a random or essentially random manner, each with a probability of 0.5.

All binary codes have the common weakness that they are quite sensitive to the Doppler shift in the received signal. Their performance degrades significantly for large Doppler frequencies. The polyphase codes exhibit better Doppler tolerance and have relatively good sidelobe characteristics. Frank codes and P4 codes are commonly used polyphase codes. They can be thought of as discrete approximations to the linear *FM* waveform.

The two devices to implement the phase-coded pulse compression are the all-range compressor and cross correlator. The former is suitable for signals with varying delays, and works well for all target range. The latter is usually used when the target range is approximately known.

## High-Resolution Radar Imaging

A radar image is the spatial distribution of microwave reflectivity corresponding to the object. Besides high range resolution, an imaging radar also requires a high azimuth resolution. It thus requires a large antenna aperture in azimuth direction. To avoid practical difficulties in constructing a large antenna, the synthetic aperture technique is developed.

**Principles of Synthetic Aperture Techniques.** The azimuth resolution of a real antenna is discussed first. Consider the linear array model of Fig. 1. For simplicity, we assumed that there is no beam steering and uniform weighting is applied to each array element, that is, $\boldsymbol{w} = [1,1,\ldots,1]^{\mathrm{T}}$. Similar to Eq. (30), the array response can be found as

$$r(\theta) = \sum_{n=0}^{N-1} \exp[-jn\phi(\theta)] = N\frac{\sin[N\pi(d/\lambda)\sin\theta]}{N\sin[\pi(d/\lambda)\sin\theta]} \qquad (70)$$

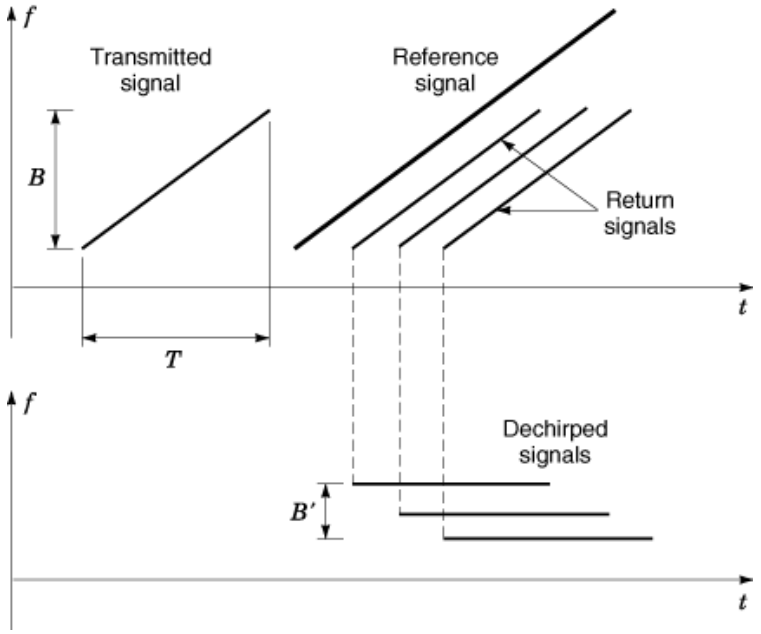


**Fig. 10.** The stretch processing can reduce the signal bandwith by dechirping the return signal. The dechirped signal is then digitized and transformed by an *FFT*, which accomplishes pulse compression.

where $\lambda = c/f$ is the wavelength. The $r(\theta)$ is also a periodic sinc function similar to Eq. (31). The peak of its mainlobe is at $\theta = 0$. Its first null occurs when $\sin\theta = \lambda/(Nd)$, where $Nd = D$ is the entire array aperture. When $D$ is very large, $\sin\theta$ is very small, and $\sin\theta \approx \theta$. So the first null occurs at $\theta = \lambda/D$. The peak–null beam width, the distance from the peak to the first null, is thus

$$\beta_\theta = \lambda/D \tag{71}$$

Although the result is derived from the array antenna, it is applicable to continuous-aperture antennas. The azimuth resolution of a real antenna at range $r$ is $R\lambda/D$ .

Synthesizing a large antenna aperture can be achieved by mounting a small-aperture antenna on a moving platform. The antenna transmits and receives signals while the platform moves. The received data can then be used to synthesize a large aperture. Such a system is called synthetic aperture radar (*SAR*).

Figure 11, shows two common operating modes of SAR: strip map and spotlight. In strip-map *SAR*, the antenna beam is fixed relative to the flight path. The moving antenna sweeps out a strip of terrain that is parallel to the flight path. In spotlight *SAR*, the beam is steered to continuously illuminate a relatively small patch of terrain. There is another widely used mode that is called inverse synthetic aperture radar (*ISAR*). In *ISAR*, the radar is usually stationary (although it can also be moving), and the target being imaged is moving. After motion compensation, the relative motion between the radar and the target is similar to that of the spotlight *SAR*.

The azimuth resolution of *SAR* can be derived from Fig. 12 by finding the synthetic-array response. The cross-range (azimuth) direction, denoted by $x$, is defined in the flight direction. *SAR* processing can be of focused or unfocused type. In focused processing, the phases of the signals are compensated so that each array element receives a signal from the origin O with the same phase. It is equivalent to transforming the linear array into

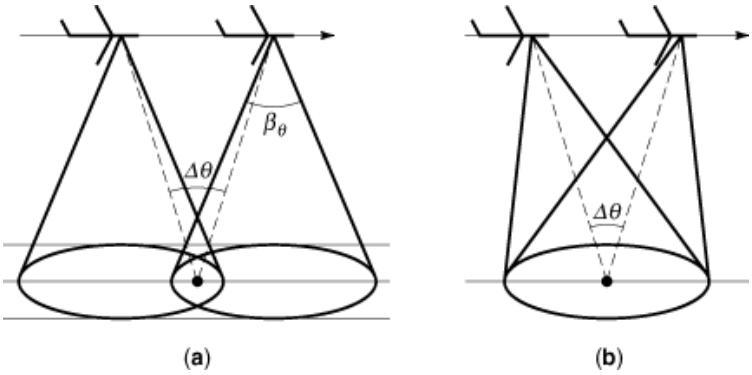


**Fig. 11.** (a) Strip-map-mode *SAR*. Its resolution is limited by the antenna beamwidth $\beta_\theta$ due to the fixed antenna pointing. (b) Spotlight-mode *SAR*. The antenna tracks a small imaging area. Its resolution can be very high, but imaging area is limited by antenna beamwidth.

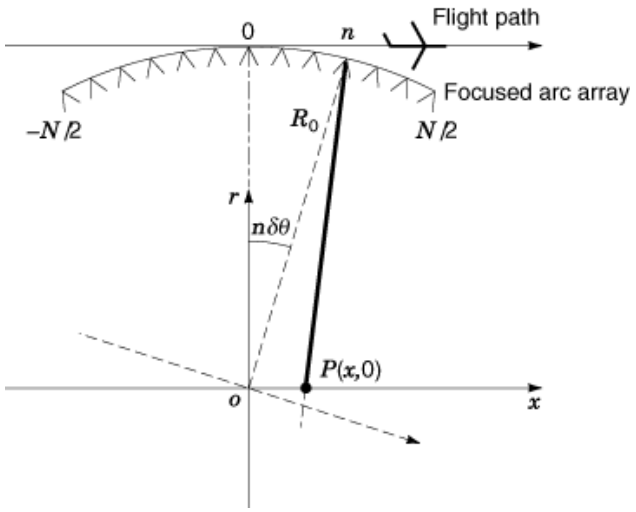


**Fig. 12.** The cross-range resolution of *SAR* can be derived from this array model. It is compensated to an arc array in the focused *SAR* processing.

an arc array. The unfocused processing does not perform such phase compensation and has a low resolution. The cross-range resolution is derived here only for focused processing.

The movement of the radar along the arc path introduces a relative rotation between the radar and the target. The observing angle from radar to the origin O will change an amount of $\delta\theta$ between two adjacent elements. Assume that there are $N$ elements in all, and the central element is the reference. The $N$th element has an observing angle of $n\delta\theta$ $(-N/2 \le n \le N/2)$ .

Denote the distance from the origin to each element on the arc array by $R_0$. Since only the cross-range resolution is of interest, we consider a point $P$ at $(x, 0)$. It is in the far field with respect to the real antenna and $x \ll R_0$. So the distance from $P$ to the $n$th element is

$$R_n(x) \approx R_0 - x \sin n\delta\theta \qquad (72)$$

The phase of the signal caused by the two-way time delay is

$$\phi_n(x) = \frac{4\pi}{\lambda} R_n(x) \approx \frac{4\pi}{\lambda} R_0 - \frac{4\pi}{\lambda} x \sin n\delta\theta \qquad (73)$$

The first term in Eq. (73) is a constant phase and can be removed. The term $n\delta\theta$ is usually very small, and thus $\sin n\delta\theta \approx n\delta\theta$. So the array response is

$$r(x) \approx \sum_{n=-N/2}^{N/2} \exp\left(-j\frac{4\pi}{\lambda} x n\delta\theta\right) = N \frac{\sin[(2\pi/\lambda)N\delta\theta x]}{(2\pi/\lambda)N\delta\theta x} \qquad (74)$$

It is a sinc function. The peak is at $x = 0$, and the first null occurs at $(2\pi/\lambda)N\delta\theta x = \pi$. So the cross-range resolution measured by the peak–null beam width is

$$\rho_x = \frac{\lambda}{2\Delta\theta} \qquad (75)$$

where $\Delta\theta = n\delta\theta$ is the total integration angle. The cross-range resolution expressed by Eq. (75) is applicable to strip-map *SAR*, spotlight *SAR*, and *ISAR*. It can also be expressed by the synthetic aperture length $L$ since $\Delta\theta = L/R_0$. Thus

$$\rho_x = \frac{\lambda R_0}{2L} \qquad (76)$$

In strip-map *SAR*, the synthetic aperture length $L$ and the integration angle $\Delta\theta$ are limited by the beamwidth of the real antenna $\beta_\theta$ due to the fixed beam steering. As shown in Fig. 11, the maximum value of $\Delta\theta = \beta_\theta$, which is expressed by Eq. (71). Therefore, the maximum cross-range resolution in strip-map *SAR* is

$$\rho_{x\max} = \frac{\lambda}{2(\lambda/D)} = \frac{D}{2} \qquad (77)$$

where $D$ is the aperture length of the real antenna.

**Strip-Map *SAR* Image Formation.** The most common method for strip-map *SAR* image formation is the range-Doppler (RD) algorithm. Consider the geometry of data collection shown in Fig. 13, where $r$ denotes the slant range and $x$ denotes the cross-range. Assume that the transmitted pulse is

$$s_t(t) = a(t)\exp\{j[\omega t - \phi(t)]\} \qquad (78)$$

where $a(t)$ is a rectangular window of unity amplitude over the pulse duration, and $\phi(t)$ represents the phase modulation. The distance from the radar to a target at $x = 0$ varies according to

$$R(x, r) = \sqrt{r^2 + x^2} \approx r + x^2/(2r) \qquad (79)$$

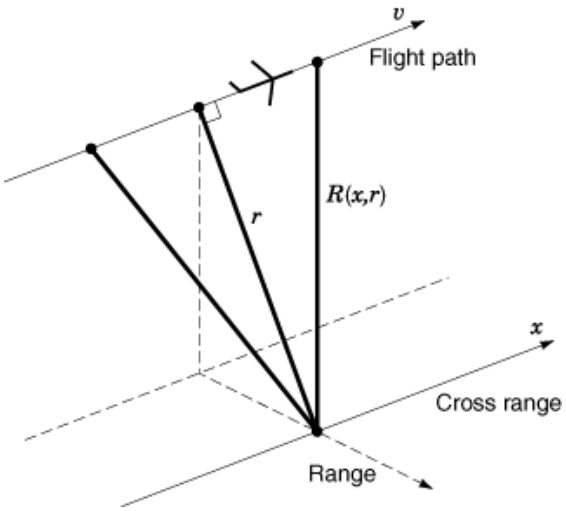


**Fig. 13.** Data collection geometry of the strip-map *SAR*.

The received signal from this point after demodulation is

$$s_r(t,x,r) = \sigma a[t-2R(x,r)/c]\exp(-j\{4\pi R(x,r)/\lambda + \phi[t-2R(x,r)/c]\}) \tag{80}$$

where $\sigma$ is the radar cross section of the target. The change of antenna gain is assumed to be small and can be omitted. The normalized form of Eq. (80) is the impulse response:

$$h(t,x,r) = a[t-2\Delta R(x,r)/c]\exp(-j\{4\pi \Delta R(x,r)/\lambda + \phi[t-2\Delta R(x,r)/c]\}) \tag{81}$$

where

$$\Delta R(x,r) = R(x,r) - r \approx x^2/(2r) \tag{82}$$

which is the well-known range migration (*RM*). *RM* can be neglected if $\beta_\theta$ is small. It is also omitted in the unfocused processing. In the focused processing, the integration of the signal must be along the curved locus, or the curved locus must be straightened (RM compensated) before integration.

The return signal from an extended target $\sigma(x, r)$ is

$$s_r(x,r) = \sigma(x,r) \otimes h(x,r) \tag{83}$$

where $\otimes$ denotes a two-dimensional convolution. It can be shown (12) that Eq. (83) can be expressed by

$$s_r(x,r) = [\sigma(x,r) \otimes h_1(x,r)] \otimes h_2(x,r) \tag{84}$$

where

$$h_1(x, r) = \delta(r - \Delta R(x, r)) \exp[-j4\pi \Delta R(x, r)/\lambda] \qquad (85)$$

$$h_2(x, r) = (2/cv)\delta(x)a(r) \exp[-j\phi(r)] \qquad (86)$$

where $v$ is the along-track speed of the radar and $\delta(\ )$ is Dirac's delta function. It can be seen that the received signal is obtained by sequentially convolving $\sigma(x, r)$ with two impulse response $h_1$ and $h_2$. Therefore $\sigma(x, r)$ can be reconstructed by sequentially correlating the return signal $s_r(x, r)$ with $h_2$ and $h_1$. Equation (86) shows that $h_2$ is actually a one-dimensional (1-D) function of range $r$, and has the same waveform as the transmitted pulse. Correlation of $s_r(x, r)$ with $h_2$ is thus the conventional pulse compression in range.

The $h_1$ is a 2-D function due to the *RM* effect. The *RM* compensation is usually implemented by an interpolation in the range-Doppler domain, which straightens the curved locus. The signal is then compressed in azimuth after the correction (12,13,14). To further reduce the phase errors, a technique called secondary range compression (13,14,15) can be adopted.

Besides the RD algorithm, two wave-number domain algorithms have also been developed for *SAR* processing: the range migration algorithm (*RMA*) (16) and the chirp scaling algorithm (*CSA*) (17). Denote the Fourier transform of $h(t, x, r)$ by $h(\omega, k_x, k_r)$, where $k_x$ and $k_r$ are spatial frequencies and are usually called $x$ and $r$ wave numbers; $\omega$ is the temporal frequency, and $k_r = 2\omega/c$.

The *RMA* first transforms the received data $s_r(x, t)$ to $s_r(k_x, \omega)$ by a 2-D Fourier transform. Then it maps the data from the $k_x - \omega$ domain to the $k_x - k_r$ domain by a process called Stolt interpolation. A 2-D phase compensation is performed in this domain, which corrects the range migration effect. The image is finally constructed by a 2-D inverse Fourier transform.

The *RMA* is capable of imaging large terrain area with fine resolutions. Its drawback is that the Stolt interpolation is time consuming. Figure 14 is an example of *SAR* image processed by the RMA. The raw data are collected by ESAR-2, and made available by German Aerospace Research Establishment (DLR). The image resolution is about 3 m in range and 0.2 m in azimuth.

The difficulty of *RM* correction is that scatterers located at different positions have different migration loci, and thus a large amount of computational effort is need. On the other hand, with its unique procedures, the chirp scaling algorithm is able to adjust all the different loci to the same trajectory in the 2-D spatial-frequency domain without much computational effort. Then the range-migration correction can be easily performed by a phase multiplication to each point.

The *CSA* requires only *FFT*s and complex multiplies. No interpolation is needed. So it is computationally efficient. However, it has been shown (18) that the *CSA* implements only the shift and linear components of the Stolt mapping. So the *RM* compensation is not complete. Nonetheless, such approximate compensation can produce satisfactory results for most applications.

**Image Formation in Spotlight *SAR* and *ISAR*.** The spotlight *SAR* and *ISAR* are developed mainly for imaging a small terrain or target with high resolutions. To take the advantage of the small imaging area, spotlight *SAR* and *ISAR* systems usually adopt the linear *FM* signal and the stretch processing technique described earlier. Stretch processing can largely reduce the analog signal bandwidth, and thus requires low AD sampling rates, and small storage memory.

Recall the principles of stretch processing depicted in Fig. 10. Here the reference signal for dechirping (mixing) process is chosen to be the replica of the return signal from the center of the scene being imaged. The return signals from the scene center after mixing have zero Doppler frequency, which means that there is no relative radial motion between the radar and the scene center. So it is also referred to as motion compensation with respect to the scene center. While this procedure compensates the translational motion, it retains the rotational motion between the radar and the scene center, which forms an ideal arc synthetic array.

**Fig. 14.** An example of an ESAR-2 strip-map *SAR* image. It is processed by the range-migration algorithm. The ESAR-2 data are made available by courtesy of the German Aerospace Research Establishment (DLR).

It can be shown (18) that the motion compensation dechirpes received signals in both range and azimuth directions and transforms the data into the $k_r - k_x$ domain. As discussed earlier, this is the two-dimensional spatial-frequency (wave-number) domain. Thus, the image can be constructed by a 2-D inverse Fourier transform. The question is that the data samples in the $k_\mathrm{r} - k_\mathrm{x}$ domain are not located on a rectangular grid. Rather, they are on the polar coordinates. The data support is a ribbon whose size is determined by the transmitted bandwidth $B$ and the integration angle $\Delta\theta$, as shown in Fig. 15.

For a small scene size, if the values of $B$ and $\Delta\theta$ are small, which means low resolutions in range and azimuth, the small ribbon can be directly approximated by a rectangle. Then the 2-D inverse Fourier transform can be performed by two 1-D inverse *FFT*s in range and azimuth. This method is referred to as a rectangular format algorithm. A scatterer can be well focused by this algorithm if it does not move through resolution cells during the whole observation. For large scene size and high resolutions, the scatterer's motion through resolution cells will cause image defocus. So the data must be stored in the polar format. Since the Fourier transform does not have fast algorithms in polar format, a 2-D interpolation is needed to map the data from polar to rectangular grid. Finally the image can be constructed via two 1-D inverse *FFT*s. This method is called polar format algorithm.

The range-migration algorithm and the chirp scaling algorithm discussed in the preceding section can be utilized for spotlight *SAR* image formation. They do not require motion compensation to the scene center. Another method known as convolution back-projection algorithm, which is widely used in computer-aided tomography (*CT*), can also be used for spotlight *SAR* image formation, since the geometry of data collection in spotlight *SAR* is very similar to that in *CT* (19).

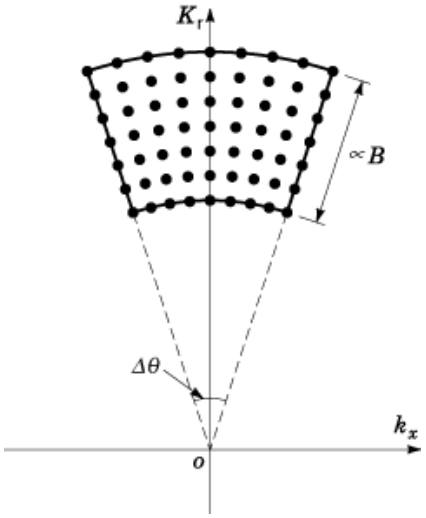


**Fig. 15.** Support area of spotlight *SAR* signals after motion compensation to the scene center. Its size is determined by the signal bandwidth and the integration angle. Data samples are located on the polar format.

**Autofocus Techniques.** Even in a well-designed *SAR* system, it is still difficult to measure the relative motion between the radar and the target with high accuracy over the whole synthetic aperture. The case is even worse in *ISAR* because the target is usually noncooperative. In such cases, phase errors will be introduced to the received signals. Such phase errors are space-invariant, which means all the range bins have the same phase error during one observation. Autofocus is a useful technique to estimate and remove the space-invariant phase errors.

Many autofocus algorithm have been presented, such as the map drift (*MD*) algorithm (18), the dominant scatterer algorithm (*DSA*) (20), the phase gradient autofocus (*PGA*) algorithm (21), and the weighted least-square (*WLS*) algorithm (22).

Autofocus usually begins in the range-compressed phase history domain, where the data are compressed in range but not compressed in azimuth. Suppose the strongest scatterer in the $n$th range bin has the Doppler frequency $f_{\mathrm{n}}$ and the initial phase $\psi_{0n}$. Other smaller scatterers are treated as clutter. So the phase of the signal at range bin $n$ and aperture position $m$ is

$$\Phi_n(m) = 2\pi f_n m + \psi_{0,n} + \phi_n(m) \qquad (87)$$

where $\phi_n(m)$ is the phase fluctuation caused by clutter. Clutter is commonly assumed independent from range bin to range bin. When corrupted by a phase error $\gamma(m)$, Eq. (87) becomes

$$\Phi_n(m) = \gamma(m) + 2\pi f_n m + \psi_{0,n} + \phi_n(m), \qquad n = 1, 2, \ldots, N \quad (88)$$

where $N$ is the number of range bins. $\gamma(m)$ is the same for all range bins, since it is space-invariant.

Autofocus is carried out in two steps: estimation and correction. The challenge is the estimation of $\gamma(m)$. Once the estimate $\hat{\gamma}(m)$ is obtained, correction can be done by multiplying the range-compressed phase history data by $\exp[-j\hat{\gamma}(m)]$.

The *WLS* algorithm is an optimal estimation of $\gamma(m)$ in the sense that it minimizes the variance of the residual phase error. It is capable of estimating and removing all kinds of phase errors, no matter if they are of

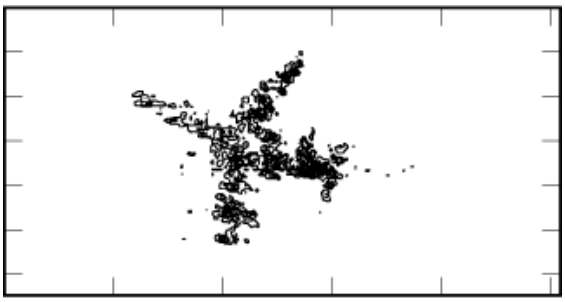

**Fig. 16.** A real *ISAR* image of an aircraft. It is autofocused by the *WLS* algorithm.

low order, high order, or entirely random. The first step in the *WLS* algorithm is to shift the strongest scatterer in each range bin to the center of the image, thus removing its Doppler frequency offset. The initial phase $\psi_{0,n}$ is a constant and can also be removed by proper processing. Then Eq. (88) becomes

$$\Phi_n(m) = \gamma(m) + \phi_n(m), \qquad n = 1, 2, \ldots, N \tag{89}$$

The task is to estimate the phase error $\gamma(m)$ from Eq. (89). Since $\phi_n(m)$ causes estimation errors, the objective of the *WLS* estimation is to minimize the variance of the estimation error. Rewriting Eq. (89) using vector notations, we have

$$\Phi(m) = H\gamma(m) + \phi(m) \tag{90}$$

where $\Phi(m) = [\Phi_1(m), \Phi_2(m), \ldots, \Phi_N(m)]^{\mathrm{T}}$, $\phi(m) = [\phi_1(m), \phi_2(m), \ldots, \phi_N(m)]^{\mathrm{T}}$, and $\boldsymbol{H} = [1, 1, \ldots, 1]^{\mathrm{T}}$.

Denote the variance of the phase term $\phi_n(m)$ by $\sigma^2{}_n$. The covariance matrix of $\phi(m)$ is

$$\boldsymbol{R} = \mathrm{diag}[\sigma_1^2, \sigma_2^2, \ldots, \sigma_n^2] \tag{91}$$

The weighted least-square estimate of $\gamma(m)$ is

$$\hat{\gamma}_{\mathrm{wls}}(m) = (\boldsymbol{H}^{\mathrm{T}}\boldsymbol{R}^{-1}\boldsymbol{H})^{-1}\boldsymbol{H}^{\mathrm{T}}\boldsymbol{R}^{-1}\Phi(m) \tag{92}$$

Figure 16 shows a real *ISAR* image of an aircraft that is autofocused by the *WLS* algorithm. The image resolution is approximately 0.4 m $\times$ 0.4 m.

The *PGA* is a widely used algorithm in *SAR* community. It has an iterative procedure for phase-error correction. The first step is the same as that in the *WLS* algorithm, that is, moving the strongest scatterer of each range bin to the image center. The second step is the windowing of each shifted image. The window is centered on the strongest scatterer. Windowing increases the *SNR* by preserving the width of dominant blur while discarding scatterers that cannot contribute to the phase-error estimation.

The next step is to estimate the phase error, or rather, the phase gradient or phase difference. Denote the range-compressed phase history data by $g_n(m) = |g_n(m)| \exp\{j[\gamma(m) + \phi_{\mathrm{n}}(m)]\}$ where $\phi_n(m)$ is the phase fluctuation caused by the clutter within the window. A linear unbiased minimum variance estimate of the

gradient of the phase error is

$$\hat{\dot{\gamma}}(m) = \frac{\sum_n \mathrm{Im}[g_n^*(m)\dot{g}_n(m)]}{\sum_n |g_n(m)|^2} \tag{93}$$

Another estimate of the phase difference is

$$\Delta\hat{\gamma}(m) = \angle[\sum_n g_n(m+1)g_n^*(m)] \tag{94}$$

where $\angle$ pian denotes the angle of the complex quantity computed on $[-\pi, \pi]$. This is a maximum likelihood estimate.

The estimated phase gradient or phase difference is integrated to obtain the estimate of phase error $\gamma\hat{}(m)$. It is used for correction after removing any bias and linear component. Then the *PGA* goes back to its first step and adopts a narrower window. The process is repeated until the image is well focused.

## Summary

This article has discussed major techniques of radar signal processing. These techniques can be divided into two categories. The first category includes the techniques for suppressing interference and enhancing the useful signal. They ensure reliable detection and processing, and are listed as follows.

- *Matched filter*. It is the optimum filter that achieves the maximum *SNR*.
- *MTI*. It discriminates moving target from fixed clutter by Doppler filtering.
- *Beam forming*. It mitigates against jamming sources by spatial filtering.
- *CFAR*. It maintains a constant false-alarm rate even if the clutter intensity varies.

The techniques in the second category are mainly developed for improving the resolving capability of radar. They enable radar to acquire complex information like target size, shape, and image.

- *Pulse compression*. It achieves high resolution in range direction without sacrificing the detection range.
- *Radar imaging.* The synthetic aperture radar is developed to attain high resolution in azimuth direction. The signal-processing techniques in *SAR* are discussed in some details, including methods for image formation, motion compensation, and autofocus.

It is foreseeable that radar will advance with the advancement of signal-processing techniques and hardware technology. It will be more robust when working in less-than-ideal environments and have stronger capability for acquiring complex information.

## BIBLIOGRAPHY

1. M. I. Skolnik *Introduction to Radar Systems*, 2nd ed., New York: McGraw-Hill, 1980.
2. J. Radatz *The IEEE Standard Dictionary of Electrical and Electronics Terms*, 6th ed., New York: IEEE, 1997.
3. D. K. Barton S. A. Leonov *Radar Technology Encyclopedia*, Boston: Artech House, 1997.
4. M. I. Skolnik *Radar Handbook*, 2nd ed., New York: McGraw-Hill, 1990.
5. S. Haykin A. Steinhardt *Adaptive Radar Detection and Estimation*, New York: Wiley, 1992.

6. B. D. Van Veen K. M. Buckley Beamforming: A versatile approach to spatial filtering, *IEEE Acoust. Speech Signal Process. Mag.*, **5** (2): 4–24, 1988.
7. L. J. Griffiths C. W. Jim An alternative approach to linearly constrained adaptive beamforming, *IEEE Trans. Antennas Propag.*, **30**: 27–34, 1982.
8. R. Nitzberg *Adaptive Signal Processing for Radar*, Boston: Artech House, 1992.
9. N. Levanon *Radar Principles*, New York: Wiley, 1988.
10. D. R. Wehner *High-Resolution Radar*, 2nd ed., Boston: Artech House, 1995.
11. F. E. Nathanson *Radar Design Principles*, 2nd ed., New York: McGraw-Hill, 1990.
12. C. Wu K. Y. Liu M. Y. Jin Modeling and a correlation algorithm for spaceborne *SAR* signals, *IEEE Trans. Aerosp. Electron. Syst.*, **18**: 563–575, 1982.
13. M. Y. Jin C. Wu A *SAR* correlation algorithm which accommodates large range migration, *IEEE Trans. Geosci. Remote Sens.*, **22**: 592–597, 1984.
14. R. Bamler A comparison of range-doppler and wavenumber domain *SAR* focusing algorithms, *IEEE Trans. Geosci. Remote Sens.*, **30**: 706–713, 1992.
15. F. H. Wong I. G. Cumming Error sensitivities of a secondary range compression algorithm for processing squinted satellite *SAR* data, *Proc. IEEE Geosci. Remote Sens. Symp. (IGARSS'89)*, Vancouver, 1989, pp. 1702–1706.
16. C. Cafforio C. Prati F. Rocca *SAR* data focusing using seismic migration techniques, *IEEE Trans. Aerosp Electron. Syst.*, **27**: 194–207, 1991.
17. R. K. Raney, *et al.* Precision *SAR* processing using chirp scaling, *IEEE Trans. Geosci. Remote Sens.*, **32**: 786–799, 1994.
18. W. G. Carrara R. S. Goodman R. M. Majewski *Spotlight Synthetic Aperture Radar: Signal Processing Algorithms*, Boston: Artech House, 1995.
19. C. V. Jakowatz Jr., *et al. Spotlight-Mode Synthetic Aperture Radar: A Signal Processing Approach*, Boston: Kluwer Academic, 1996.
20. C. C. Chen H. C. Andrews Target-motion-induced radar imaging, *IEEE Trans. Aerosp. Electron. Syst.*, **16**: 2–14, 1980.
21. D. E. Wahl, *et al.* Phase gradient autofocus—A robust tool for high resolution *SAR* phase correction, *IEEE Trans. Aerosp. Electron. Syst.*, **30**: 827–835, 1994.
22. W. Ye T. S. Yeo Z. Bao Weighted least square estimation of phase errors for SAR/ISAR autofocus, *IEEE Trans. Geosci. Remote Sens.*, **37**: 2487–2494, 1999.

WEI YE
TAT SOON YEO
National University of Singapore